Energy & Environmental Science

Accepted Manuscript

ROYAL SOCIETY OF CHEMISTRY

www.rsc.org/ees

Cite this: DOI: 10.1039/c0xx00000x

www.rsc.org/xxxxxx

ARTICLE TYPE

High Efficiency Hybrid PEDOT:PSS/Nanostructured Silicon Schottky Junction Solar Cells by Doping-Free Rear Contact

Yunfang Zhang,[a,b] Wei Cui,[a] Yawen Zhu,[a] Fengshuo Zu,[a] Liangshen Liao,[a] Shuit-Tong Lee,[a] Baoquan Sun*[a]

Received (in XXX, XXX) Xth XXXXXXXXX 20XX, Accepted Xth XXXXXXXXX 20XX
DOI: 10.1039/b000000x

A high doping technique has been widely used for record-efficiency crystalline silicon (Si) solar cells to minimize the series resistance losses and to form a back surface field. However, it requires high temperatures (up to 1000 °C) and involves toxic gases, which may not be compatible for hybrid organic-silicon solar cells. Here, we report that a high power conversion efficiency (PCE) of 13.7% with a device area of 0.8 cm^2 has been achieved for organic-nanostructured Si hybrid solar cells by inserting a cesium carbonate (Cs_2CO_3) layer between Si and rear electrode aluminium (Al), which is realized by a solution process under low-temperature annealing (<150 ℃). Transient and constant current-voltage, capacitance-voltage, and scanning Kelvin probe microscope measurements are used to characterize the effect of the Cs_2CO_3 layer on the device performance. The insertion of Cs_2CO_3 not only decreases the contact resistance, but also generated a built-in electric field on the rear electrode. The recombination rates are suppressed at the back surface due to the deflection of minority carriers. These findings show a promising strategy to achieve high performance organic-silicon solar cells with a simple, low temperature and cost effective process.

Introduction

Transparent conducting polymer/silicon (Si) hybrid Schottky solar cells have attracted wide research interests due to their simple device structure compared with Si-based traditional p-n junction photovoltaics.[1-10] One of the most important advantages of organic-Si hybrid solar cells is that it allows the stacking of different materials without the severe requirements on lattice matching in Si heterojunctions. Poly(3,4-ethylenedioxythiophene) /poly(styrenesulfonate) (PEDOT:PSS) has been extensively investigated for the hybrid solar cells due to its high transparency and conductivity.[9, 11-13] Various approaches have been made to enhance the performance of this kind of the devices, such as Si surface passivation,[10, 14-16] surface morphology controlling[3, 9, 11, 13, 17-19] and property tuning of PEDOT:PSS.[4, 7, 20-22] A power conversion efficiency (PCE) of over 13% has been achieved for the PEDOT:PSS/Si solar cells.[8, 23 24]In addition, carbon nanotubes (CNTS)-Si heterojunction photovoltaics with efficiencies up to 15% by coating a TiO_2 antireflection layer and doping CNTs with oxidative chemicals as transparent window have been demonstrated. [25] However, to the best of our knowledge, there has hardly been any investigation on rear electrode, which plays a critical role on device performance.[2, 3] Generally, the cathode is either Ga:In eutectic, aluminum (Al) or Ti/Pd/Ag.[8, 10, 11] The physical mechanism of the rear electrode has not been a popular topic of research for the hybrid solar cells.[2, 3, 18]

Traditionally, the Si-metal ohmic contact is synthesized by highly p- or n-doping at high temperatures (up to 1000 °C)[26] to form the back surface field. This process requires the use of hazardous doping gases, such as diborane (B_2H_6) and phosphine (PH_3), which poses operational and environmental issues. Doping has a detrimental effect on the quality of crystalline Si because it results in the creation of additional Si dangling bonds. Due to the high temperatures required and the complicated process, the doping method may be not compatible for organic-Si hybrid solar cells.

Cesium carbonate (Cs_2CO_3) has been used as an effective electron-injection (and hole-blocking) layer at the cathode interface in organic devices.[27, 28] This is mainly ascribed to the decreased work function (WF) of Cs_2CO_3/Al due to Cs_2CO_3 decomposing into cesium oxide (Cs_2O) when annealed.[29] In addition, an Al-O-Cs structure is formed when thermally evaporating Al, which further lowers the WF of Al.[28] A solution fabrication process can be used to avoid any physical and chemical stresses at the interface, thus leading to better junction properties.[30]

Here, we develop an alternative back contact method by inserting a Cs_2CO_3 layer between the rear side of n-Si and Al for a Si/PEDOT:PSS solar cell. Nanostructured Si is used to increase the light harvesting capability. When the Cs_2CO_3 layer is inserted between nanostructured Si and the rear electrode Al, a high PCE of 13.7% is achieved, which is a 27% improvement in comparison to a Si/Al direct contact device (PCE: 10.8%).

Experimental section

Preparation of nanostructured Si

The nanostructured Si was prepared by a metal ion-assisted electroless chemical etching process.[31] Planar Si substrates (n-type Si (100)) with resistivity of 0.05~0.1 Ω•cm were immersed in a solution of hydrofluoric acid (HF) (4.8 M) and silver nitride

($AgNO_3$) (0.02 M) at room temperature for 5 min. Then they were rinsed with deionized water and dipped in a nitric acid (HNO_3) solution. To reduce surface/volume ratio, the substrates were immersed in a solution of HF (4.8 M) for 10 min and anisotropic tetramethyl ammonium hydroxide (TMAH)/DI water (V/V=1:25) for 30 s.

Device fabrication

Cs_2CO_3 and polyethylenimine (PEI) were dissolved in 2-methoxyethanol with a concentration of 0.5 mg/mL and 1 mg/mL, respectively. A Cs_2CO_3/PEI (V/V=1:1) mixture solution was spin coated onto the rear of nanostructured Si substrates and then annealed with infrared radiation for 20 min. A highly conductive PEDOT:PSS (CLEVIOS PH 1000) solution mixed with 5 wt.% dimethyl sulfoxide (DMSO) and 1 wt.% Triton (from Aldrich) was spin-coated onto the front side of the nanostructured Si substrates. Then, the substrates were annealed at 125 ^oC for 30 min in a nitrogen atmosphere. A silver grid electrode was deposited on top of the PEDOT:PSS layer through a shadow mask. A 150-nm-thick Al film was deposited onto the rear Si substrates by thermal evaporation (Mini-SPECTROS, Kurt J. Lesker Co.). The active area of the device was 1 cm × 0.8 cm.

Device characterization

The photovoltaic characterization was conducted in ambient condition. A Newport 91160 solar simulator equipped with a 300 W xenon lamp and an air mass (AM) 1.5 filter were used to generate a simulated solar spectrum irradiation source. The irradiation intensity was 100 mW/cm^2, which was calibrated with a Newport Si solar cell 91150. A Newport monochromator 74125 and power meter 1918 with a Si detector 918D were used in the external quantum efficiency (EQE) measurement. All of the electrical data were recorded by a Keithley 2612 source meter. Capacitance versus voltage (C–V) measurement was carried out with a Wayne Kerr 6500B impedance analyzer. Reflection spectrum was measured by a spectrometer (Perkin-Elmer Lambda 750) with an integrating sphere. Morphology and scanning Kelvin probe microscopy (SKPM) were characterized with an atomic force microscopy (AFM, Veeco, Multimode V). The nanostructured Si was characterized with a high-resolution scanning electron microscope (SEM) (Carl Zeiss, Supra 55). Optical microscope images were obtained from a fluorescence optical microscope (Laica, DM4000M). Regarding to the transient electric output characteristic setup, the devices were connected to a digital oscilloscope with an input impedance of 1 MΩ. The intensity of white light, which was referred to hereon as a "light bias", was used to control the open-circuit voltage (V_{oc}) of the devices. A laser with a wavelength of 532 nm was used as optical perturbation, pulse duration was set to 1 μs and frequency was set to 100 Hz, which resulted in a voltage transient with a peak value of 10 mV ($<<V_{oc}$). The frequency, light intensity and pulse duration were kept constant, with the photocurrent transient at an impedance of 50 Ω.

Results and discussion

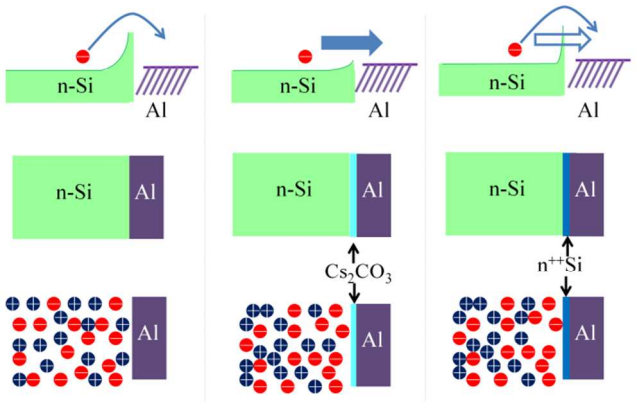

Fig. 1 Energy alignment and electron/hole distribution of (a) Si/Al; (b) Si/Cs_2CO_3/Al; (c) Si/n^{++}Si/Al under illumination. For Si directly contacts with Al in (a), there is a large energy barrier for electrons to be collected by the Al electrode. The electron and hole concentrations are equal at the rear interface of Al and Si. After inserting a Cs_2CO_3 layer to make (b) Si/Cs_2CO_3/Al, the effective barrier is reduced due to the lowering of the work function of Al. In traditional (c) Si/n^{++}Si/Al devices, the barrier is only slightly reduced, generally tunnelling effect is dominant.

The organic-inorganic hybrid device was generally assumed to be a Schottky junction between n-Si, PEDOT:PSS, and the rear electrode.[32] PEDOT:PSS acted as a window electrode, which allowed light to reach Si. The PEDOT:PSS film displayed good light transparency (300-1100 nm, >90%) with high conductivity (up to 1000 S·cm^{-1}).[33] In order to improve hole collection efficiency, a silver grid electrode was deposited onto the PEDOT:PSS film. PEDOT:PSS with a WF of ~5.1 eV[33] was used for hole collection and Al as the rear metal for electron collection. Light was harvested by the Si substrate and a built-in electric field was formed in Si to sweep the charges towards the proper direction. For the rear contact of the most hybrid organic-silicon devices, a metal layer (e.g. Al) is directly deposited on Si,[7] as shown in **Figure 1(a)**. In an ideal metal-semiconductor Schottky barrier, the barrier height was mainly determined by the properties of the metal and the metal-semiconductor interface. For Si, the barrier height was nearly independent of doping concentration. There was a large energy barrier between Al and Si, electrons have to pass through this barrier to be collected by Al. In addition, there was an equal amount of electrons and holes at the Si interface, and charge recombination become a serious issue. If the rear contact was ohmic, then the electrons could be effectively collected by Al and total charge recombination is minimized. A few methods were used to tune the barrier height of metal and silicon interface.[26] Traditionally, a thin highly doped layer (<10 nm) was incorporated, and the effective barrier height for a given metal-semiconductor interface was tuned, as shown in **Figure 1(c)**. For the contact with a thin n^{++}Si layer, the barrier was dramatically reduced due to tunneling effect. In addition, an electric field was formed at the rear interface, which suppressed holes that flow to the rear surface. The hole concentration was thus maintained at higher levels in the bulk of the device and the recombination velocity decreased. Cs_2CO_3 was inserted between Si and Al in order to decrease the barrier height, as shown in **Figure 1(b)**. In addition, charge recombination was also suppressed, which was similar to a thin n^{++}Si layer. A device without Cs_2CO_3 was used as a reference.

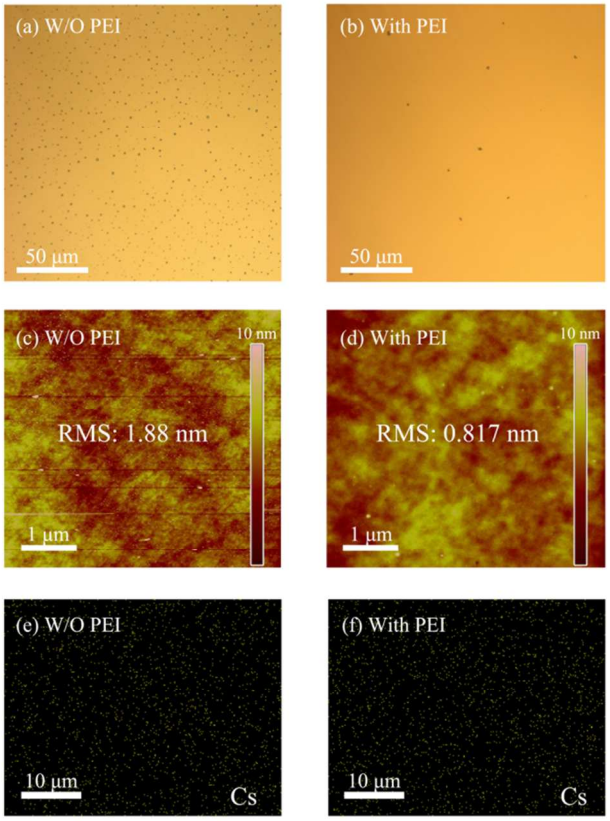

Fig. 2 Optical microscope images (a) without PEI, (b) with PEI; AFM images of the Cs_2CO_3 film (c) without PEI, (d) with PEI on Si, the inset figures in (c) and (d) show the RMS values, respectively; and the element mapping images by energy-dispersive X-ray spectroscopy of cesium (e) without PEI, (f) with PEI.

Pristine Cs_2CO_3 was unable to form a continuous film on a Si substrate through a spin-coating process. As shown in the optical microscope images in **Figure 2 (a),** large particles were formed due to Cs_2CO_3 re-crystallization during the spin-coating process. The film displayed a discontinuous layer (shown in the AFM images in **Figure 2 (c))**, and therefore, uncovered regions still existed where Al could still directly contact with Si. The film quality was dramatically improved when PEI was added to the Cs_2CO_3 solution, which was shown in **Figure 2 (b) and (d)**. Surface roughness of the both films was characterized by AFM in terms of root-mean-square (RMS) roughness. PEI, which exhibited a high number of amine groups (the chemical structure of PEI was shown in **Figure S1**), displayed excellent dispersion properties in a methoxyethanol solution. The incorporation of PEI formed a uniform film with RMS value of 0.817 nm extracted from AFM image, while the film based on pristine Cs_2CO_3 displayed a rather rough surface with RMS value of 1.88 nm. Also, it assured that Cs_2CO_3 formed a uniform dispersion on the Si substrate, which was confirmed by energy-dispersive X-ray spectroscopy of cesium, as shown in **Figure 2 (e)** and **(f)**. There was almost no difference between **Figure 2 (e)** and **(f),** which indicated that the dispersion of Cs_2CO_3 almost did not change after PEI addition. The energy-dispersive X-ray spectroscopy of carbon was also measured and shown in **Figure S2**. The concentration of carbon increased with PEI addition, which was ascribed to the carbon source of PEI. Once Al was deposited on the uniform Cs_2CO_3 layer, a mild annealing treatment would lead to form Cs-O-Al complex.[29]

The devices were fabricated to explore the effect of the Cs_2CO_3 interlayer on the rear contact. As compared to planar Si, nanostructured Si displayed much lower light reflectance, which should dramatically improve the light harvest capability. The reflectance spectra of planar Si and nanostructured Si coated with PEDOT:PSS were shown in **Figure S3,** where nanostructured Si exhibited average ~15% reflection ratio while planar one displayed 25% reflection ratio. The morphology of the nanostructured Si (**Figure S4)** revealed that the antireflection was provided by the graded index of refraction in the nanostrucute.

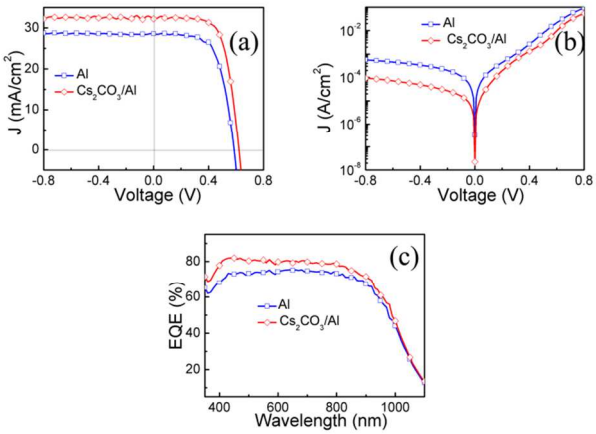

Fig. 3 Current density versus voltage characteristic of the hybrid solar cells with and without Cs_2CO_3 under (a) 100 mW/cm^2 illumination (AM 1.5G), (b) dark; (c) EQE spectrum of the hybrid solar cells with and without Cs_2CO_3.

Current versus voltage (J-V) curves of the hybrid solar cells with and without Cs_2CO_3 under simulated AM 1.5 illuminations at 100 mWcm^{-2} were shown in **Figure 3 (a)**. The photovoltaic parameters of the short circuit current density (J_{sc}), the V_{oc}, the fill factor (FF) and the PCE of the hybrid solar cells with and without Cs_2CO_3 layer and their statistics (of seven cells for each type) were summarized in **Table 1**. The champion device with the Cs_2CO_3 layer exhibited the highest FF of 68.4%, an V_{oc} of 0.621 V, a J_{sc} of 32.2 mAcm^{-2} and a record PCE of 13.7%. The reference device (direct contact of Si and Al) with an V_{oc} of 0.586 V, a J_{sc} of 28.6 mAcm^{-2}, a FF of 64.9% yielded a PCE of 10.8%. The inserted Cs_2CO_3 layer resulted in a 27% PCE enhancement compared with the reference device. The EQE spectra were measured, as shown in **Figure 3 (c)**. The device with the interlayer displayed higher EQE values in the visible and near infrared region when compared with the reference device, which was in line with the enhanced J_{sc} value.

In order to quantify the improvements in device performance after inserting the Cs_2CO_3 layer between nanostructured Si and Al, detailed measurements, including constant and transient output characteristics and Kelvin scanning microscopy were conducted in the following sections.

Cite this: DOI: 10.1039/c0xx00000x

www.rsc.org/xxxxxx

ARTICLE TYPE

Table 1. Electron output characteristics of the hybrid solar cells with and without Cs_2CO_3 layer.

Rear Electrode[a)]	V_{oc} [b)] (V)	J_{sc} [b)] ($mAcm^{-2}$)	FF [b)] (%)	PCE [b)] (%)	R_s [b)] ($\Omega \cdot cm^2$)
Al	**0.586**	**28.6**	**64.9**	**10.8**	**3.46**
	0.585(±0.007)	28.5(± 0.7)	63.5 (±1.28)	10.5 (±0.3)	3.42(±0.3)
Cs_2CO_3/Al	**0.621**	**32.2**	**68.4**	**13.7**	**2.16**
	0.624(±0.003)	31.4 (±0.9)	68.8 (±1.14)	13.4 (±0.6)	2.03(±0.7)

[a)] Data and statistics based on seven cells of each condition; [b)] Numbers in bold are the maximum record values.

Figure 3 (b) showed the J-V characteristics of the hybrid solar cells with and without Cs_2CO_3 in dark. It was observed that saturation current density (J_s) was suppressed significantly after the Cs_2CO_3 layer was inserted between Si and Al. The dark J-V curves were simulated according to the thermionic emission model.[34] The J_s was obtained by fitting

$$J = J_s\left(\exp\left(\frac{qV}{nkT}\right)-1\right)$$

where J is the current density value, V is the applied voltage, T is the absolute temperature (298 K), k is the Boltzmann constant (1.38×10^{-23} m^2 kg s^{-2} K^{-1}), and q is the electronic charge (1.6×10^{-19} C)). The device without Cs_2CO_3 displayed a J_s value of 1.8×10^{-8} A/cm^2. The device with Cs_2CO_3 exhibited a J_s of 1.4×10^{-9} A/cm^2. The J_s decreased ~15 times and the V_{oc} increased ~40 mV when the Cs_2CO_3 layer was incorporated. The suppressed J_s was ascribed to a reduced contact barrier by inserting the Cs_2CO_3 layer. The device with a lower J_s led to a larger V_{oc} according to the photovoltaic general relation:

$$V_{oc} = \frac{nkT}{q}\ln\left(\frac{J_{sc}}{J_s}\right)$$

The contact between Al and the rear side of Si was dramatically improved using the Cs_2CO_3 layer. Al pads were deposited onto Si through thermal evaporation. According to J-V measurements, shown in **Figure 4 (a)**, it revealed that the contact between Si and Al was non-ohmic. A transmission line measurement (TLM) was conducted to measure the contact resistance.[35] The detailed TLM method was described in Electronic Supporting Information (ESI). Schematic diagram for measuring the contact resistance value was shown in **Figure S5**. The contact resistance was 3.97×10^{-1} $\Omega\cdot cm^2$ for the Al/Si direct contact. A non-ohmic contact resulted in a high contact resistance between Si and the rear electrode Al, which led to charge accumulation at the rear electrode interface. A highly doped layer was used for an improved contact in the traditional Si solar cell, where the contact resistance was reduced to 10^{-2}-10^{-3} $\Omega\cdot cm^2$.[2,35] The highly doped layer also significantly lowered saturation current density (to as low as 10^{-13} A/cm^2) and enhanced the V_{oc}.[36] Here, with the insertion of the Cs_2CO_3 layer between Si and Al, the current-voltage curve was linear, as shown in **Figure 4 (a)**, which indicated an improved contact. The contact resistance was 6.18×10^{-2} $\Omega\cdot cm^2$ when the Cs_2CO_3 layer was inserted, which was similar in value to the contact resistance when the high temperature and highly doped process was used. The series resistance (R_s) was extracted from the plot of dV/d(lnJ) versus J (the detailed derivation process was described in ESI). **Figure 4(b)** showed the dV/d(lnJ) versus J curves of the hybrid solar cell, with and without the Cs_2CO_3 layer. The device with and without Cs_2CO_3 layer displayed R_s values of 2.16 $\Omega\cdot cm^2$ and 3.46 $\Omega\cdot cm^2$, respectively, as shown in **Table 1**. The value of R_s decreased after inserting the Cs_2CO_3 layer, which was consistent with the improved back contact.

The insertion of the Cs_2CO_3 layer not only decreased the contact resistance but also generated a larger built-in electric field on the rear electrode. This deflected minority carriers and recombination rates were suppressed at the back surface. The $1/C^2$-V plots at signal frequency of 1 KHz of the hybrid solar cells with and without Cs_2CO_3 were shown in **Figure 4(c)**. C was the capacitance of the device. Here, $1/C^2$ was linear with the applied voltage and the intercept corresponded to the built-in potential. The devices with the Cs_2CO_3 layer yielded a higher built-in potential than the reference one. A higher built-in potential effectively deflected electrons from migrating towards the cathode.

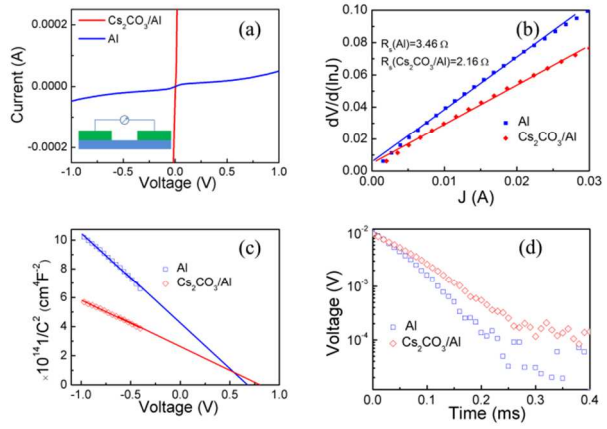

Fig. 4 (a) Current-voltage measurements between the T-shaped Al pads deposited by thermal evaporation at the rear side of Si with and without the Cs_2CO_3 layer; (b) Series resistance values were extrapolated from dV/d(lnJ) versus J curves of the hybrid solar cells with and without the Cs_2CO_3 layers. (c) $1/C^2$-V plots of the hybrid solar cells with and without the Cs_2CO_3 layer; (d) Photovoltage decay measurements on the device with and without the Cs_2CO_3 layer.

The improved rear contact and increased built-in potential were ascribed to the Al WF dropping in the presence of the Cs_2CO_3 layer. The WF change was measured by SKPM in ambient conditions.[37, 38] Since our devices were characterized in ambient air, the SKPM technique should be suitable to interpret the WF change. The same conductive tip was used during the entire measurement to ensure that its WF remained constant. The relationship between the WF of the conductive tip, Φ_t, and the samples, Φ_s, is given by

$$\Phi_s = \Phi_t - eV_{sp}$$

where e is the elementary charge and V_{sp} is the surface potential measured by SKPM. A higher surface potential corresponds to a lower WF of the measured sample. As shown in **Figure 5**, the surface potential of Cs_2CO_3/Al decreased when compared with bare Al. This result was consistent with previous measurements made by ultraviolet photoemission spectrum (UPS) in a high vacuum[28,29], where a strong chemical reaction occurred between Cs_2CO_3 layer and thermally evaporated Al. In the thermal evaporation process, the first layer of Al atoms formed chemical bonds with the underlying Cs_2CO_3 layer. Metallic Al could only be detected after deposing a second Al layer determined by X-ray photoelectron spectroscopy. Many O atoms bonded to both Al and Cs atoms in the Al-O-Cs complexes, which was critical in reducing the WF of Al. And the decreased WF of Al reduced the Schocky barrier height, as shown in **Figure 1(b)**. As a result, the built-in potential increased, which would reduce charge carrier recombination.

The charge carrier recombination kinetics at open circuit conditions can be explored by transient photovoltaic measurements according to previous reports.[39-41] In order to be consistent with the J-V test, the background light intensity was set to 100 $mWcm^{-2}$. The transient photovoltage (TPV) decay was fitted with a mono-exponential decay equation

$$\delta V = \Delta V_0 \exp(-t/\tau)$$

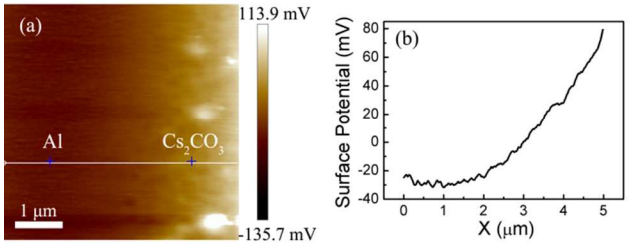

Fig. 5 Using SKPM to probe the potential difference of Cs_2CO_3 and Al. (a) Surface potential images. (b) Cross-section line profile of the surface potential image

where ΔV_0 is a constant that fits to the peak height (10 mV), t is the decay time and τ is the carrier lifetime. A steady state of electron and hole concentration and a stable V_{oc} were achieved under illumination. The concentration of electrons and holes started to decrease as a result of recombination when the illumination was turned off. The decay of V_{oc} revealed charge carriers recombination in the hybrid device. **Figure 4(d)** showed transient photo-voltage as a function of time for the devices with and without Cs_2CO_3. The reference device showed a charge carrier lifetime of 53.7 μs, while the champion device with Cs_2CO_3 displayed longer carrier lifetime of 73.6 μs. This result indicated the insertion of the interlayer between Si and cathode suppressed the carrier recombination and lower saturation current, both the J_{sc} and the V_{oc} were improved.

Conclusion

In conclusion, we developed a dopant-free rear contact for high performance organic-inorganic polymer/nanostructured Si solar cells. The rear contact was fabricated by inserting a solution processed Cs_2CO_3 layer between nanostructured Si and Al. A champion PCE of 13.7% was achieved by this simple and low temperature process (<150 ^oC). The superior device performance was ascribed to the reduced WF of Al with the Cs_2CO_3 layer, which resulted in the suppression of the saturation current density, reduced contact resistance and enhancement of the built-in potential. The improvement of the rear contact allowed the minority carrier to be deflected, leading to the suppression of carrier recombination. This simple, low temperature fabrication process for the hybrid solar cell promises low cost photovoltaics.

Acknowledgement

This work was supported by the National Basic Research Program of China (973 Program) (2012CB932402), National Natural Science Foundation of China (91123005, 61176057, 61211130358), Jiangsu Key Laboratory for Carbon-Based Functional Materials & Devices, the Priority Academic Program Development of Jiangsu Higher Education Institutions and Collaborative Innovation Center of Suzhou Nano Science and Technology. We would appreciate Mr. Tam Jasper for the very detailed paper reading and correction.

Notes and references

[a] *Institute of Functional Nano & Soft Materials (FUNSOM, Soochow University, 199 Ren'ai Road, Suzhou, 215123, Jiangsu, People's Republic of China; E-mail: bqsun@suda.edu.cn*

[b] *Department of Mathematics and Physics, Jiangsu University of Science and Technology, Zhenjiang, 212003, People's Republic of China*

†Electronic Supplementary Information (ESI) available: method for extraction of contact resistance, method for extracting series resistance, PEI chemical structure, element mapping images by energy-dispersive X-ray spectroscopy of carbon with and without PEI, reflectance of planar Si and nanostructured Si coated with PEDOT:PSS, SEM image of the nanostructured Si, schematic diagram for measuring the contact resistance value. See DOI: 10.1039/b000000x/

1. M. J. Sailor, E. J. Ginsburg, C. B. Gorman, A. Kumar, R. H. Grubbs and N. S. Lewis, *Science*, 1990, **249**, 1146-1149.
2. Y. Zhang, F. Zu, S. T. Lee, L. Liao, N. Zhao and B. Sun, *Adv. Energy Mater.*, 2014, **4**, 1300923.
3. S. Jeong, E. C. Garnett, S. Wang, Z. Yu, S. Fan, M. L. Brongersma, M. D. McGehee and Y. Cui, *Nano Lett.*, 2012, **12**, 2971-2976.
4. I. Khatri, Z. Tang, Q. Liu, R. Ishikawa, K. Ueno and H. Shirai, *Appl. Phys. Lett.*, 2013, **102**, 063508.
5. S. Avasthi, S. Lee, Y. L. Loo and J. C. Sturm, *Adv. Mater.*, 2011, **23**, 5762-5766.

6. S. C. Shiu, J. J. Chao, S. C. Hung, C. L. Yeh and C. F. Lin, *Chem. Mater.*, 2010, **22**, 3108-3113.
7. J. P. Thomas, L. Y. Zhao, D. McGillivray and K. T. Leung, *J. Mater. Chem. A,* 2014, **2**, 2383-2389.
8. P. Yu, C. Y. Tsai, J. K. Chang, C. C. Lai, P. H. Chen, Y. C. Lai, P. T. Tsai, M. C. Li, H. T. Pan, Y. Y. Huang, C. I. Wu, Y. L. Chueh, S. W. Chen, C. H. Du, S. F. Horng and H. F. Meng, *ACS Nano*, 2013, **7**, 10780-10787.
9. L. He, D. Lai, H. Wang, C. Jiang and Rusli, *Small*, 2012, **8**, 1664-1668.
10. L. He, C. Jiang, H. Wang, D. Lai and Rusli, *Appl. Phys. Lett.*, 2012, **100**, 073503.
11. W. R. Wei, M. L. Tsai, S. T. Ho, S. H. Tai, C. R. Ho, S. H. Tsai, C. W. Liu, R. J. Chung and J. H. He, *Nano Lett.*, 2013, **13**, 3658-3663.
12. T. G. Chen, B. Y. Huang, H. W. Liu, Y. Y. Huang, H. T. Pan, H. F. Meng and P. Yu, *ACS Appl. Mater. Interfaces*, 2012, **4**, 6857-6864.
13. T. G. Chen, B. Y. Huang, E. C. Chen, P. Yu and H. F. Meng, *Appl. Phys. Lett.*, 2012, **101**, 033301.
14. F. Zhang, B. Sun, T. Song, X. Zhu and S. Lee, *Chem. Mater.*, 2011, **23**, 2084-2090.
15. D. Liu, Y. Zhang, X. Fang, F. Zhang, T. Song and B. Sun, *Electron Dev. Lett., IEEE*, 2013, **34**, 345-347.
16. M. Y. Bashouti, M. Pietsch, G. Brönstrup, V. Sivakov, J. Ristein and S. Christiansen, *Prog. Photovolt: Res. Appl.,* 2013, **22**,1050-1061.
17. H. Jeong, H. Song, Y. Pak, I. K. Kwon, K. Jo, H. Lee and G. Y. Jung, *Adv. Mater.*, 2014, **26**, 3445-3450.
18. J. Schmidt, V. Titova and D. Zielke, *Appl. Phys. Lett.*, 2013, **103,**183901.
19. K. Sato, M. Dutta and N. Fukate, *Nanoscale*, 2014, **6**, 6092-6101.
20. Q. Liu, M. Ono, Z. Tang, R. Ishikawa, K. Ueno and H. Shirai, *Appl. Phys. Lett.*, 2012, **100**, 183901-183904.
21. M. Pietsch, M. Y. Bashouti and S. Christiansen, *J. Phys. Chem. C*, 2013, **117**, 9049-9055.
22. D. Chi, B. Qi, J. Wang, S. Qu and Z. Wang, *Appl. Phys. Lett.*, 2014, **104**, 193903.
23. J. P. Thomas and K. T. Leung, *Adv. Funct. Mater.*, 2014, **24**,4978-4985.
24. R. Liu, S. T. Lee and B. Sun, *Adv. Mater.*, 2014, **26**, 6007-6012.
25. E. Shi, L. Zhang, Z. Li, P. Li, Y. Shang, Y. Jia, J. Wei, K. Wang, H. Zhu and D. Wu, *Sci. Rep.*, 2012, **2**, 884.
26. S. M. Sze and K. K. Ng, *Physics of Semiconductor Devices*, Wiley-interscience, 2006.
27. J. Huang, G. Li, E. Wu, Q. Xu and Y. Yang, *Adv. Mater.*, 2006, **18**, 114-117.
28. J. Huang, Z. Xu and Y. Yang, *Adv. Funct. Mater.*, 2007, **17**, 1966-1973.
29. H. H. Liao, L. M. Chen, Z. Xu, G. Li and Y. Yang, *Appl. Phys. Lett.*, 2008, **92**, 173303.
30. M. Nakano, A. Tsukazaki, R. Gunji, K. Ueno, A. Ohtomo, T. Fukumura and M. Kawasaki, *Appl. Phys. Lett.*, 2007, **91**, 142113.
31. K. Q. Peng, Y. J. Yan, S. P. Gao and J. Zhu, *Adv. Mater.*, 2002, **14**, 1164-1167.
32. M. J. Price, J. M. Foley, R. A. May and S. Maldonado, *Appl. Phys. Lett.*, 2010, **97**, 083503.
33. Y. Xia, K. Sun and J. Ouyang, *Adv. Mater.*, 2012, **24**, 2436-2440.
34. X. Li, H. Zhu, K. Wang, A. Cao, J. Wei, C. Li, Y. Jia, Z. Li and D. Wu, *Adv. Mater.*, 2010, **22**, 2743-2748.
35. G. Reeves and H. Harrison, *Electron Dev. Lett., IEEE*, 1982, **3**, 111-113.
36. J. Nelson, The physics of Solar Cell. Imperial College Press, London, 2003,.
37. L. Sun, J. Wang and E. Bonaccurso, *J. Phys. Chem. C*, 2010, **114**, 7161-7168.
38. V. Palermo, M. Palma and P. Samorì, *Adv. Mater.*, 2006, **18**, 145-164.
39. A. H. Ip, S. M. Thon, S. Hoogland, O. Voznyy, D. Zhitomirsky, R. Debnath, L. Levina, L. R. Rollny, G. H. Carey and A. Fischer, *Nat. Nano.*, 2012, **7**, 577-582.
40. Z. Li, F. Gao, N. C. Greenham and C. R. McNeill, *Adv. Funct. Mater.,* 2011, **21**, 1419-1431.
41. C. Shuttle, B. ORegan, A. Ballantyne, J. Nelson, D. Bradley, J. De Mello and J. Durrant, *Appl. Phys. Lett.*, 2008, **92**, 093311-093313.

Graphical Abstract

A champion PCE of 13.7% has been achieved by inserting a solution processed Cs_2CO_3 layer between nanostructured Si and Al.